Supplementary Materials of

Hydrogen sulfide at high-pressure: a strongly-anharmonic phonon-mediated superconductor

Ion Errea[1,2], Matteo Calandra[3],* Chris J. Pickard[4], Joseph Nelson[5], Richard J. Needs[5], Yinwei Li[6], Hanyu Liu[7], Yunwei Zhang[8], Yanming Ma[8], and Francesco Mauri[3]

[1]*Donostia International Physics Center (DIPC), Manuel de Lardizabal pasealekua 4, 20018 Donostia-San Sebastián, Basque Country, Spain*

[2]*IKERBASQUE, Basque Foundation for Science, Bilbao, Spain*

[3]*IMPMC, UMR CNRS 7590, Sorbonne Universités - UPMC Univ. Paris 06, MNHN, IRD, 4 Place Jussieu, F-75005 Paris, France*

[4]*Department of Physics & Astronomy, University College London, Gower Street, London WC1E 6BT, UK*

[5]*Theory of Condensed Matter Group, Cavendish Laboratory, J J Thomson Avenue, Cambridge CB3 0HE, UK*

[6]*School of Physics and Electronic Engineering, Jiangsu Normal University, Xuzhou 221116, People's Republic of China*

[7]*Department of Physics and Engineering Physics, University of Saskatchewan, Saskatchewan S7N 5E2, Canada and*

[8]*State Key Laboratory of Superhard Materials, Jilin University, Changchun 130012, People's Republic of China*

*matteo.calandra@upmc.fr

A. Technical details of the structural searching

The structure searches were performed using the CALYPSO and AIRSS codes, and the results were combined to produce the final data. Searches were performed at 200, 250, and 300 GPa, and 44 stoichiometries were investigated:
H_2S_3 H_4S HS_3 H_4S_3 HS_4 H_2S HS_2 H_8S_3 S HS H H_7S_4 H_8S_5 HS_6 H_3S_7 H_7S_3 H_3S_4 H_3S_5 HS_5 H_5S H_3S H_6S H_8S_7 H_7S H_8S H_3S_8 H_5S_2 H_5S_3 H_5S_8 HS_7 H_5S_4 H_2S_7 H_7S_5 H_6S_5 H_7S_2 HS_8 H_4S_5 H_7S_6 H_2S_5 H_7S_8 H_5S_7 H_6S_7 H_3S_2 H_9S_2

In the CALPYSO calculations each generation contained 40 structures, and the first generation was produced randomly with symmetry constraints. All structures were locally optimized using density functional theory and the Perdew-Burke-Ernzerhof (PBE) [1] generalized gradient approximation implemented in the Vienna *ab initio* simulation package [2, 3]. An energy cutoff of 700 eV and a Monkhorst-Pack Brillouin zone sampling grid with a resolution of 0.5 $Å^{-1}$ were used in the structure searches. 60% of the lowest-enthalpy structures from each generation were used to produce the structures in the next generation using the CALYPSO particle-swarm optimisation technique, and the structural diversity was further enhanced by choosing the remaining 40% of structures using symmetry constraints. Typically, the structure searching simulations for each composition were stopped when ∼1000 successive structures were generated without finding a new lower-energy structure. Distinct low-enthalpy structures were then re-optimized using denser Brillouin zone sampling with a resolution of better than 0.2 $Å^{-1}$ and a higher energy cutoff of 1000 eV.

The AIRSS searches were performed using a wide range of stoichiometries, the PBE functional and the CASTEP code. The initial structures were obtained by selecting random cell volumes and shapes and adding atoms at random positions. The cells and atomic positions were then relaxed to minimise the enthalpy at the chosen fixed pressures. The minimum initial separations between the H–H, H–S, and S–S atomic pairs were constrained using data obtained from short AIRSS runs. Constraining the minimum separations of atomic pairs in the initial structures helps to space out the atoms appropriately, while retaining a high degree of randomness. We also constrained the symmetries of the structures to reduce the size of the "structure space" that is searched, which is useful because low energy structures very often possess symmetry. A range of different symmetry constraints was employed to allow a diverse set of structures.

B. Convex hull at 300 GPa

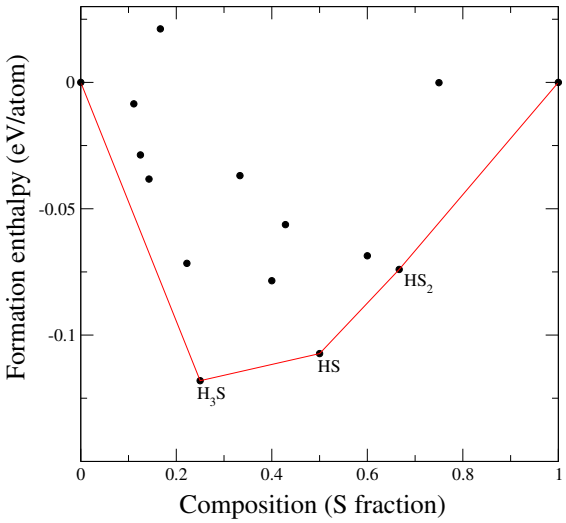

FIG. 1: Results of structural searches at 300 GPa. The continuous line shows the convex hull.

C. Effect of the zero point energy on the D_2S convex hull at 200 GPa

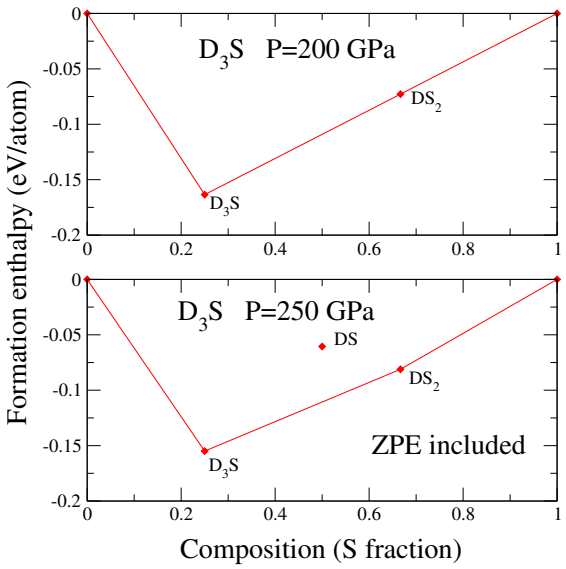

FIG. 2: Results of structural searches at 200 and 250 GPa for D-S structures including zero point energy. The continuous lines show the convex hull.

D. Crystal structures for H and S

The crystal structure for Hydrogen is from Ref. [5]. The crystal structure for S is from Ref. [6].

E. Crystal structures of HS_2 at 200, 250 and 300 GPa

TABLE I: Crystallographic data for HS_2 at 200, 250 GPa as obtained from structural searches. At 250 and 300 GPa, HS_2 adopts the same C2/m structure as at 250 GPa.

Structure	Pressure (GPa)	Structural parameters (Å, deg.)	Atomic Positions			
C2/c	200	a=6.7827, b=4.1876, c=7.5401	S	8f	0.07702	0.12708 0.42711
		$\alpha = 90$, $\beta = 137.7464$, $\gamma = 90$	S	8f	0.89224	0.37399 0.79574
			H	8f	0.28345	0.86882 0.42463
C2/m	250	a=7.2073, b=2.947, c=3.6324,	S	4i	0.33820	0.5 0.51566
		$\alpha = 90$, $\beta = 60.2287$,$\gamma = 90$	S	4i	0.59068	0.0 0.14405
			H	4i	0.61860	0.5 0.94147

The HS_2 crystal structures found with the CALYPSO and AIRSS codes are shown in Table I.

F. Crystal structures of HS and at 200, 250 and 300 GPa

TABLE II: Crystallographic data for HS at 200 and 300 GPa as obtained from structural searches. At 250 GPa and 300 GPa, HS adopts the same C2/m structure.

Structure	Pressure	Structural parameters				
			Atomic Positions			
$I4_1/amd$	200	a=b=2.9399, c=9.0531	S	16h	0.0	0.0 0.27894
			H	16h	0.5	0.0 0.62786
C2/m	300	a=9.4579, b=2.7388, c=2.749,	S	4i	0.41556	0 0.83415
		$\alpha = 90$, $\beta = 73.1325$, $\gamma = 90$	S	4i	0.33437	0.5 0.41585
			H	4i	0.00217	0.0 0.24756
			H	4i	0.25205	0.5 0.99709

G. Crystal structure of H_3S at 200 and 250 GPa

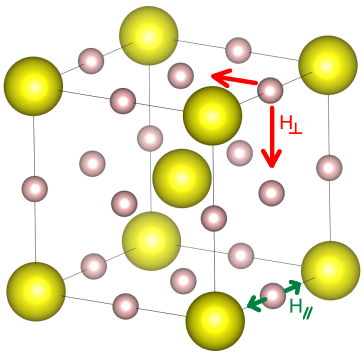

FIG. 3: Crystal structure of H_3S at 200 and 250 GPa. Hydrogen is depicted in purple while sulfur is in yellow. The red (green) arrows label the H–S bond-bending (-stretching) modes, labeled $H_\perp$ ($H_\parallel$). The volumes at 200 and 250 are 13.3334 Å^3, and 12.4925 Å^3, respectively.

H. Electronic structure of H_3S at 200 GPa

The electronic structure of H_3S at 200 GPa is shown in Fig. 5 in the *fat-bands* representation including decomposition into H and S atomic states. In a 20 eV energy window around

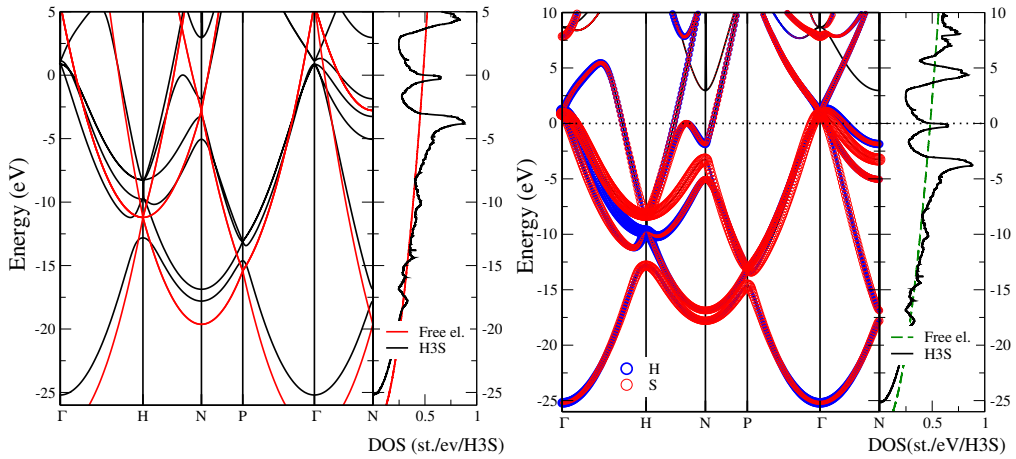

FIG. 4: Left: Free-electron bandstructure and density of states calculated for a bcc lattice with the same lattice parameter as H_3S at 200 GPa. The electronic structure and density of states of H_3S at 200 GPa are also shown for comparison. Right: Electronic structure of H_3S. The thickness of the band is proportional to the projection of the electronic state over a chosen atomic orbital (fat bands representation).

the Fermi level (ϵ_f), the electronic structure can be fairly well interpreted in terms of free electrons on a bcc lattice. However, in the proximity of the Fermi level, there is a substantial hybridization between the H and S electronic states, leading to avoided crossings at special points N, Γ and along the H-N high symmetry direction. The hybridization results in a peak in the density of states at approximately 0.17 eV below ϵ_f. At precisely ϵ_f, the density of states per spin is $N(0) = 0.33$ states/eV/spin/H_3S cell, which is essentially identical to the free-electron value.

The Fermi surface is composed of 5 sheets. The avoided crossing at the zone center generates three hole pockets centered at Γ and a cubical electron Fermi surface centered at the N point. Finally, an additional large Fermi surface sheet arises from the electron-pocket at H.

I. Vibrational and superconducting properties of D_3S at 200 GPa

The phonon dispersion of D_3S calculated using harmonic linear response theory and the stochastic self-consistent harmonic approximation is shown in Fig. 6.

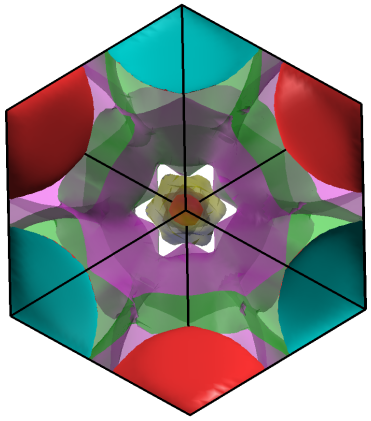

FIG. 5: Fermi surface of H_3S at 200 GPa including 5 sheets (right). The hole pockets at Γ are visible in the center. The large Fermi surface contributing most of the density of states is shown in transparent colors.

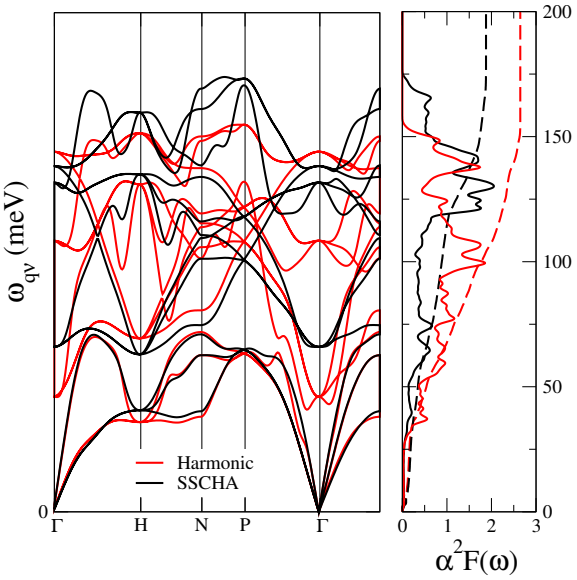

FIG. 6: Phonon spectrum, Eliashberg function and integrated electron-phonon coupling of D_3S at the harmonic and anharmonic levels (SSCHA).

J. Vibrational and superconducting properties of H_3S at 250 GPa

The phonon dispersion of D_3S calculated using harmonic linear response theory and the stochastic self-consistent harmonic approximation are shown in Fig. 7.

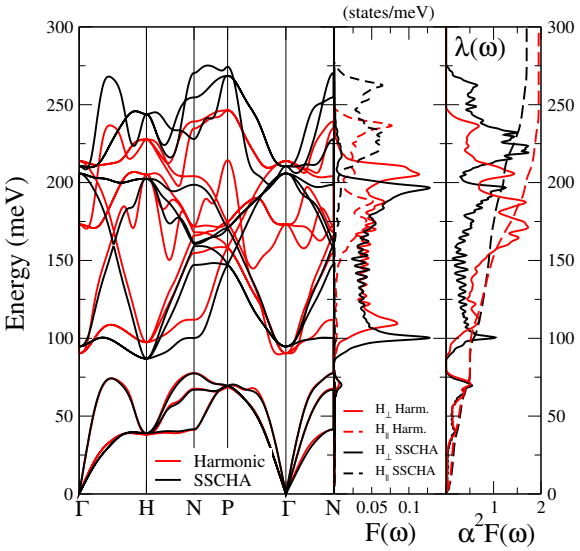

FIG. 7: Phonon spectrum, phonon density of states projected onto selected vibrations and the Eliashberg function and integrated electron-phonon coupling of H_3S at 250 GPa at the harmonic and anharmonic levels (SSCHA).

K. Migdal-Eliashberg

We solve the Isotropic Migdal-Eliashberg (ME) equations using either the harmonic Eliashberg function or the one calculated within the SSCHA. The equations are solved in the Matsubara frequency space using 512 Matsubara frequencies. The superconducting gap is obtained from the lowest Matsubara gap $\Delta_{n=0} = \Delta$ and is plotted in Fig. 8.

L. Superconducting properties using different approximations

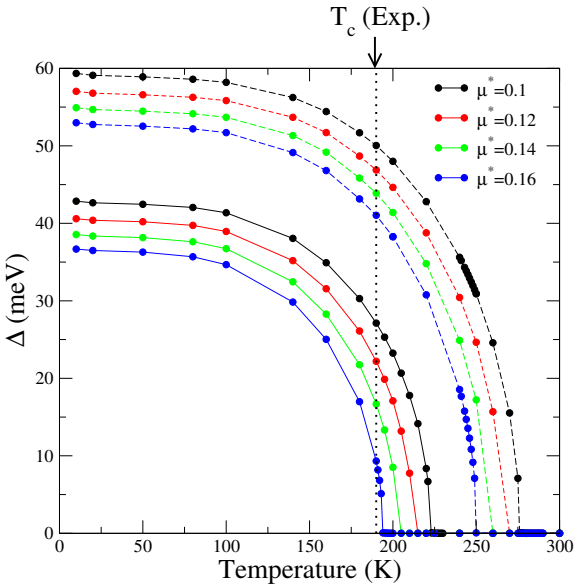

FIG. 8: Superconducting gap (Δ) as a function of temperature from the solution of the isotropic Migdal-Eliashberg equations applied to H_3S. The continuous lines refer to anharmonic phonon (SSCHA) while the harmonic phonon are denoted by dashed lines.

M. Effects of the vibrational energy on the pressure

In Fig. 9 the contribution of the atomic vibrations to the total energy is shown in the quasiharmonic approximation and SSCHA. The ground state total energy, without the zero point energy (ZPE), is fitted to a second order polynomial as a function of the volume V, $E_0(V) = A_0 + B_0 V + C_0 V^2$. The fitting parameters are reported in Table IV. We add the vibrational contribution to $E_0(V)$ calculated in the quasiharmonic approximation and in the

TABLE III: Electron-phonon interaction and a logarithmic average of phonon frequencies using the SSCHA, and without anharmonic effects. The T_cs are calculated using the SSCHA phonon spectrum and with either the McMillan equation (T_C^{MM}) or by solving the isotropic Migdal-Eliashberg equations (T_c^{ME}). A value of $\mu^* = 0.16$ is used.

Compound	λ^{har}	ω_{log}^{har} (meV)	λ^{anh}	ω_{log}^{anh} (meV)	$T_c^{MM,har}$	$T_c^{MM,anh}$	$T_c^{ME,har}$	$T_c^{ME,anh}$	T_c(Exp)
H_3S (200 GPa)	2.64	90.4	1.84	92.86	158.8	124.9	250	194.0	190
H_3S (250 GPa)	1.96	109.1	1.71	101.3	155.25	127.2	226	190	
D_3S (200 GPa)	2.64	68.5	1.87	73.3	120.4	100.3	183	152.0	90

SSCHA. This contribution is calculated at two volumes, those shown in the right panel of Fig. 9. The vibrational energy E_v is fitted linearly to $E_v(V) = A_v + B_v V$. As shown in Fig. 10, the linear fit provides a very good approximation to $E_v(V)$. The linear form of $E_v(V)$ is obtained within the quasiharmonic approximation for H_3S and D_3S, and in the SSCHA for H_3S. The ZPE energy is obtained using a 6×6×6 phonon mesh.

The correction to the pressure from including the atomic vibrations is calculated from the $E(V) = E_0(V) + E_v(V)$ curves and $P(V) = -\mathrm{d}E(V)/\mathrm{d}V$. These curves are shown in Fig. 9. Neglecting the ZPE underestimates the pressure. The correction to the pressure from the ZPE is smaller for D_3S than for H_3S due to the smaller ZPE of deuterium. The SSCHA gives a small correction to the pressure obtained within the quasiharmonic approximation. The pressure corrections to the volumes for which the electron-phonon calculations were performed are summarized in Table V.

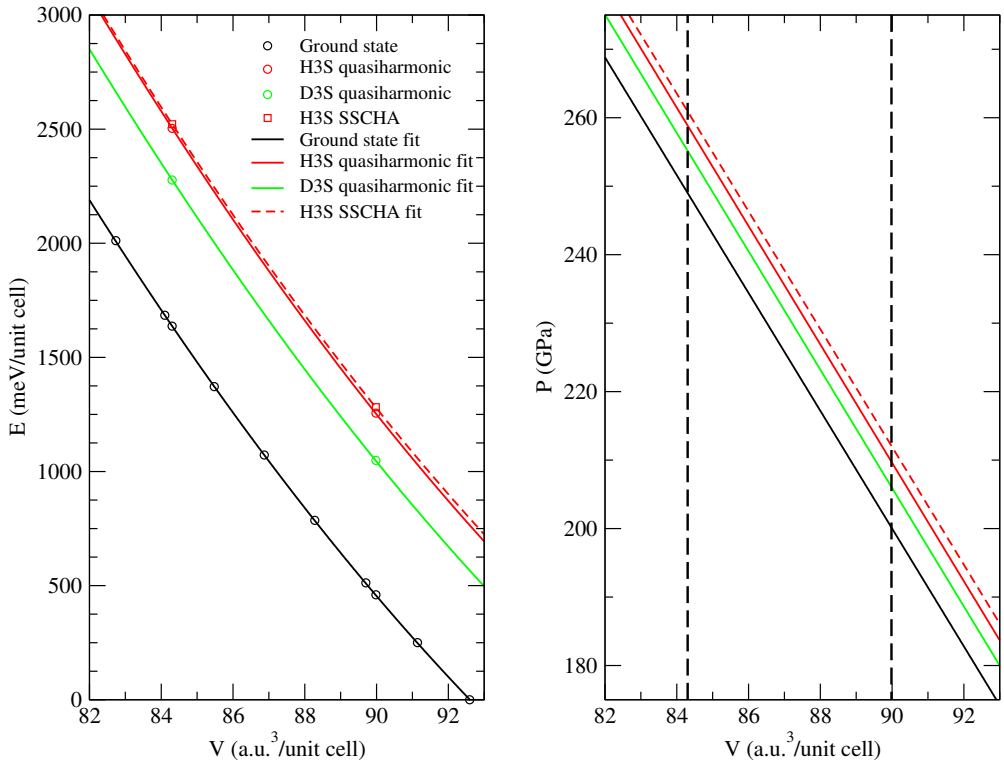

FIG. 9: (Left panel) Ground state energy without ZPE, including ZPE at the quasiharmonic level, and at the SSCHA level. The lines represent fitted curves following the recipe described in Sec. M. (Right panel) The pressure derived from the fitted energy curves. The vertical dashed lines denote the volumes used in the SSCHA calculations.

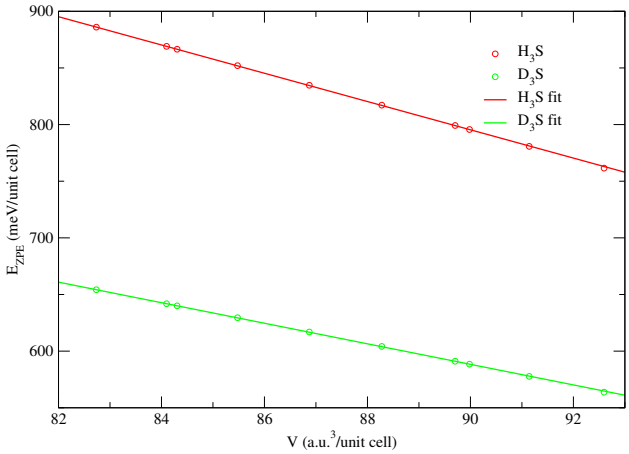

FIG. 10: ZPE calculated within the quasiharmonic level for H_3S and D_3S. The solid lines denote the linear fit obtained with two data points, the volumes are those from the right panel of Fig. 9.

N. Electronic, vibrational, and superconducting of other predicted sulfur hydrides

Here we described the electronic, vibrational, and superconducting properties of the other sulfur hydrides predicted in this study. In particular, we focus on $C2/c$ HS_2 at 200 GPa, $C2/m$ HS_2 at 250 GPa, and $C2/m$ HS at 300 GPa. The pseudopotentials, exchange-correlation kernels, plane-wave cutoff energies, and Hermitian-Gaussian smearing were the same as those used for cubic H_3S. The electronic integrations for calculating the phonon spectra within linear response were performed on a 12×8×12 mesh for $C2/c$ HS_2 at 200 GPa, a 18×15×18 mesh for $C2/m$ HS_2 at 250 GPa, and a 16×16×16 mesh for $C2/m$ HS at 300 GPa. The phonon spectrum was calculated on a 4×2×4 grid of **q** points for $C2/c$ HS_2

TABLE IV: Calculated parameters for the quadratic fit of $E_0(V)$ and the linear fit of $E_v(V)$.

	A_0 (mev)	B_0 (meV/a.u.^{3})	C_0 (meV/a.u.^{6})
	49319	-900.88	3.9772
	A_v (mev)	B_v (meV/a.u.^{3})	
H_3S quasiharmonic	1918.5	-12.479	
D_3S quasiharmonic	1404.7	-9.0707	
H_3S SSCHA	1814.2	-11.027	

at 200 GPa, a 4×3×4 grid for $C2/m$ HS_2 at 250 GPa, and a 4×4×4 grid for $C2/m$ HS at 300 GPa. In order to obtain converged electron-phonon linewidths a finer electron-phonon grid was used in the calculations: a 36×24×36 for $C2/c$ HS_2 at 200 GPa, a 45×35×45 for $C2/m$ HS_2 at 250 GPa, and a 48×48×48 for $C2/m$ HS at 300 GPa.

In Fig. 11 we show the density of states (DOS) for HS_2-$C2/c$ at 200 GPa, HS_2-$C2/m$ at 250 GPa, and HS-$C2/m$ at 300 GPa. As it can be seen, all structures are metallic. The states that dominate at the Fermi level are S p states.

The phonon spectra, phonon density of states (PDOS), Eliashberg function $\alpha^2F(\omega)$, and integrated electron-phonon coupling constant $\lambda(\omega)$ of these structures are shown in Fig. 12. These are calculated exclusively in the harmonic approximation. For all cases S and H modes are clearly separated by a large energy gap. In the HS_2 compounds the H modes are Einstein-like modes that show a very weak dispersion in the BZ. For the HS compound at 300 GPa the dispersion of the optical modes is larger. There is no instability in any of the structures and, thus, they are dynamically stable. The $\lambda(\omega)$ curve indicates that in these cases, contrary to cubic H_3S, the electron-phonon coupling constant is dominated by S atoms.

TABLE V: Correction to the pressure P from the vibrational energy.

V (a.u.^{3})	P (GPa)			
	no ZPE	D_3S quasiharmonic	H_3S quasiharmonic	H_3S SSCHA
89.9822	200	206	210	212
84.3035	250	255	259	261

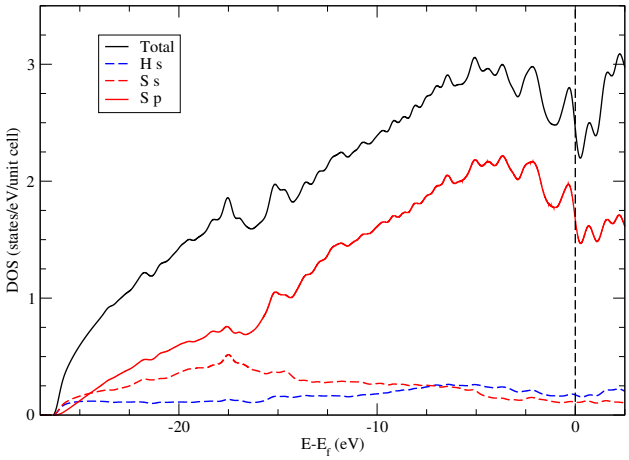

(a) $C2/c$ HS_2 at 200 GPa

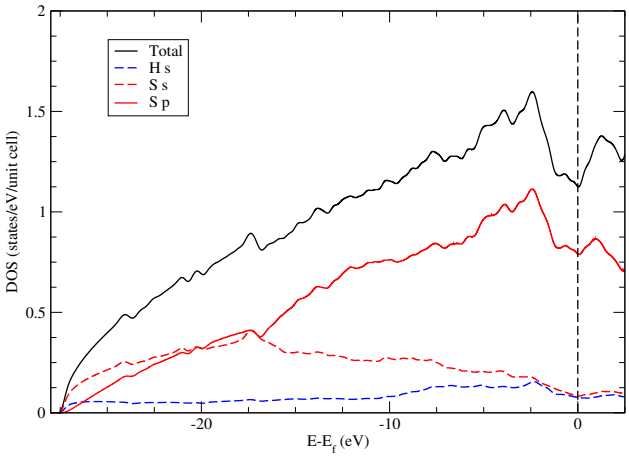

(b) $C2/m$ HS_2 at 250 GPa

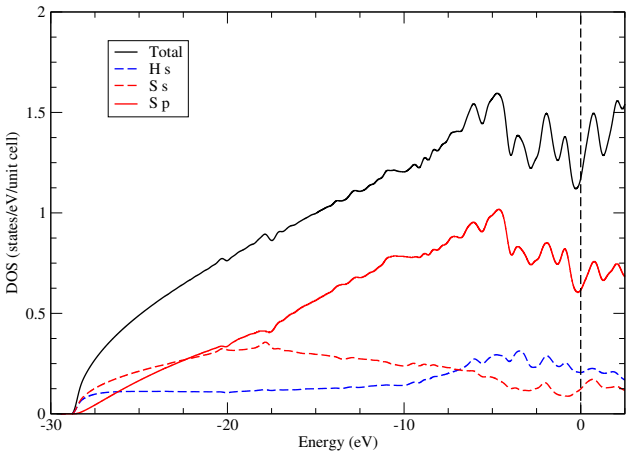

(c) $C2/m$ HS at 300 GPa

FIG. 11: DOS projected onto different atoms and angular momentum channels for the predicted hydrogen sulfides.

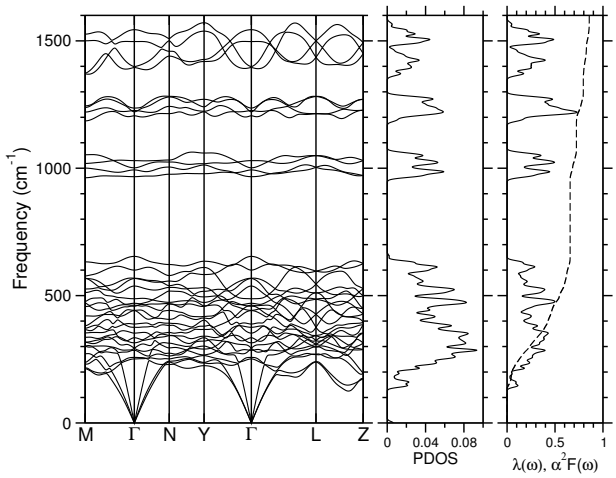

(a) $C2/c$ HS_2 at 200 GPa

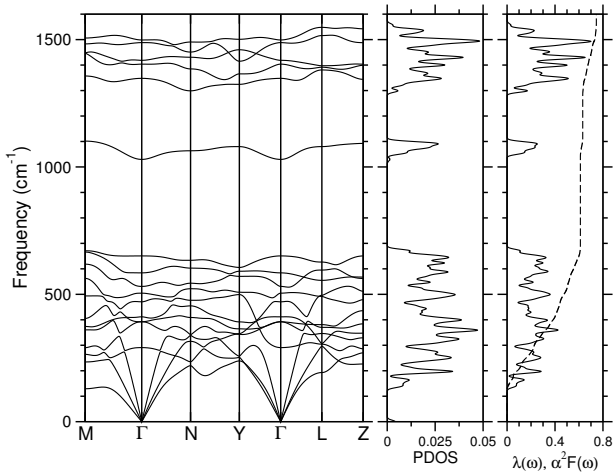

(b) $C2/m$ HS_2 at 250 GPa

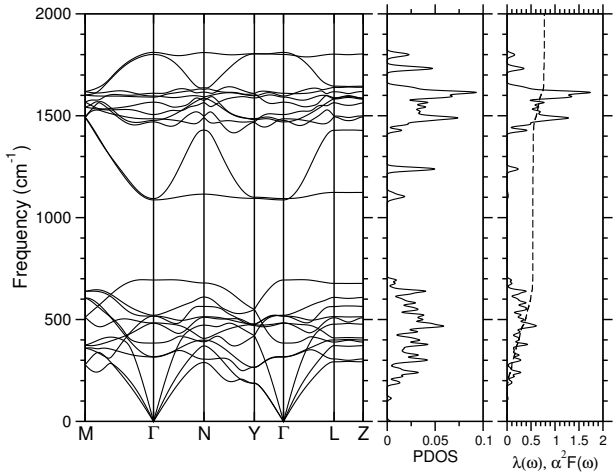

(c) $C2/m$ HS at 300 GPa

FIG. 12: (Left panel) Phonon spectra, (middle panel) PDOS, (right panel) $\alpha^2F(\omega)$ (solid line) and $\lambda(\omega)$ (dashed line) for the predicted hydrogen sulfides.

[1] J. P. Perdew, K. Burke, and M. Ernzerhof, Phys. Rev. Lett. **77**, 3865 (1996).

[2] G. Kresse and J. Furthmüller, Comput. Mat. Sci. **6**, 15 (1996).

[3] G. Kresse and J. Furthmüller, Phys. Rev. B **54**, 11169 (1996).

[4] A. Togo, F. Oba, and I. Tanaka, Phys. Rev. B **78**, 134106 (2008).

[5] C. J. Pickard and R. J. Needs, Nature Physics **3**, 473 (2007).

[6] Olga Degtyareva, Eugene Gregoryanz, Maddury Somayazulu, Ho-kwang Mao, and Russell J. Hemley, Phys. Rev. B **71**, 214104 (2005).